Mobility enhancement in strained *p*-InGaSb quantum wells

Brian R. Bennett,[a] Mario G. Ancona, J. Brad Boos, and Benjamin V. Shanabrook
Electronics Science and Technology Division, Naval Research Laboratory, Washington, DC 20375

(Received 4 April 2007; accepted 29 June 2007; published online 25 July 2007)

Quantum wells of InGaSb clad by AlGaSb were grown by molecular beam epitaxy. The InGaSb is in compressive strain, resulting in a splitting of the heavy- and light-hole valence bands and an enhancement of the mobility. The mobility was found to increase with increasing InSb mole fraction for values of strain up to 2%. Room-temperature mobilities as high as 1500 $cm^2/V\,s$ were reached for 7.5 nm channels of $In_{0.40}Ga_{0.60}Sb$. These results are an important step toward the goal of high-performance *p*-channel field-effect transistors for complementary circuits operating at extremely low power. © *2007 American Institute of Physics*. [DOI: 10.1063/1.2762279]

Over 20 years ago, the first high-electron-mobility transistors (HEMTs) were reported. Since then, both GaAs- and InP-based HEMTs have exhibited excellent high-frequency performance. In recent years, several groups have also reported progress in InAs- and InSb-channel HEMTs.[1] Because of their small band gaps and high electron mobilities, these semiconductors offer high-speed performance at much lower power. For example, low-noise amplifiers using InAs-channel HEMTs operate at frequencies of 10–100 GHz. They consume three to ten times less power than comparable InP- or GaAs-based circuits.[1] Recently, there has been interest in the potential of III-V field-effect transistors (FETs) for advanced logic applications which could enhance digital circuit functionality and extend Moore's law.[2] For these applications, a key to low power operation is the ability to make complementary circuits. In III-V materials, one challenge centers on maximizing the hole mobility in *p*-channel FETs.[3]

In the late 1980s, the use of strain to reduce hole effective masses by splitting the heavy-hole (hh) and light-hole (lh) valence bands was proposed and demonstrated in *p*-channel InGaAs/(Al)GaAs quantum wells.[4–6] FETs with *p*-InGaAs channels were also reported.[3,7] More recently, the technique has been applied to strained Ge layers on lattice-relaxed SiGe buffer layers. Room-temperature mobilities greater than 2000 $cm^2/V\,s$ have been reported for Ge.[8,9] For this work, we employ a similar strategy with the goal of demonstrating a narrow-band-gap channel material with relatively high hole mobilities. InGaSb was chosen as the channel material for two primary reasons. The first is that the valence band offset with AlGaSb will provide confinement of the holes in the channel. The second is that the strain of InGaSb can be controlled by adjusting the composition. Earlier work on *p*-GaSb and *p*-InGaSb for FET channels was reported with room-temperature mobilities ranging from 180 to 780 $cm^2/V\,s$.[10–12]

The heterostructures studied here are grown by molecular beam epitaxy (MBE) on semi-insulating GaAs and typically include a 200 nm GaAs buffer layer, a 1.5 μm $Al_yGa_{1-y}Sb$ buffer layer, a 5.0–12.5 nm $In_xGa_{1-x}Sb$ channel, a 21 nm $Al_yGa_{1-y}Sb$ barrier, and a 5 nm $Al_yGa_{1-y}Sb$(Be) modulation-doping layer. The final layers consist of a 4 nm $In_{0.2}Al_{0.8}Sb$ etch-stop layer, and a 2 nm InAs cap or a single 5 nm $Al_yGa_{1-y}Sb$ layer. Values of y were 0.7 and 0.8. Values of x will be discussed later. A calculated band structure is shown in Fig. 1. The growth temperature is near 580 and 500 °C for the GaAs and AlGaSb buffer layers, respectively. The temperature is then reduced to 450 °C for the channel and subsequent layers. The channel layers were grown at a rate near 0.5 ML/s; other layers were grown at 1.0 ML/s. The AlGaSb buffer layer fully accommodates the 8% lattice mismatch; the $In_xGa_{1-x}Sb$ channel is in biaxial compression. For a buffer layer of $Al_{0.75}Ga_{0.25}Sb$, the in-plane pseudomorphic strain associated with the lattice mismatch between the $In_xGa_{1-x}Sb$ channel and buffer layer is given by

$$\varepsilon = 0.00491 - 0.0626x.$$

In Fig. 2 results are plotted of 6×6 $k\cdot p$ calculations, performed using the NEXTNANO device simulation program (see www.nextnano.de) for the in-plane dispersion of $In_xGa_{1-x}Sb$. The figure shows the highest energy lh and hh bands for three cases: bulk, $x=0.23$ (unstrained); 7.5 nm quantum well, $x=0.23$ (1% biaxial compressive strain); and 7.5 nm quantum well, $x=0.41$ (2% biaxial compressive strain). As seen, increasing compression causes a larger splitting between the hh and lh bands with the hh band being higher in energy and hence with greater occupancy. Because hh and lh mixing is reduced near the center of the Brillouin zone, the in-plane mass of the hh band gets lighter as the hh-lh splitting increases. This reduced mass is expected to result in higher mobility.

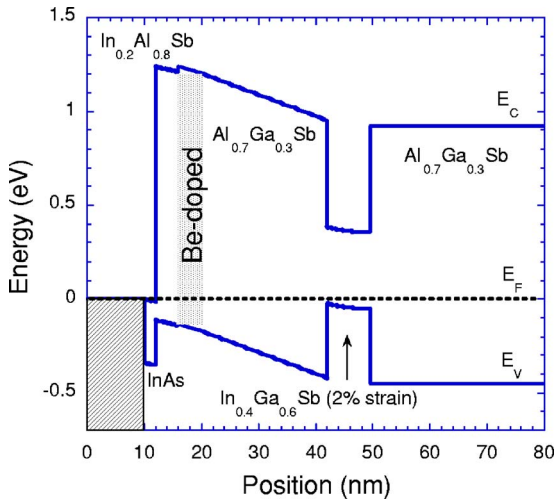

FIG. 1. (Color online) Calculated band diagram for a structure with a 7.5 nm $In_{0.40}Ga_{0.60}Sb$ channel.

[a]Electronic mail: brian.bennett@nrl.navy.mil

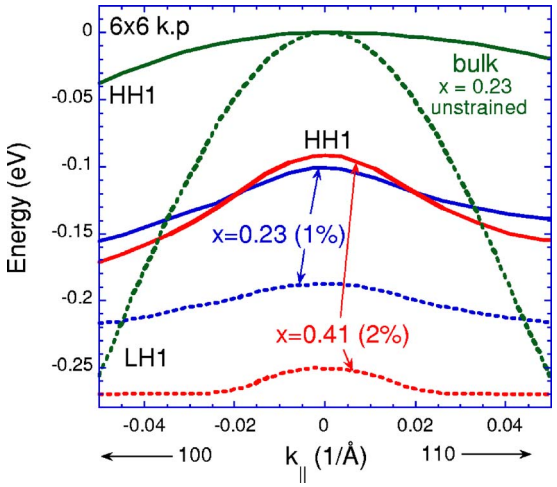

FIG. 2. (Color online) Calculated dispersion curves for InGaSb (see text).

We grew a series of six samples with a fixed quantum well thickness (12.5 nm) and varying x (0.12–0.50). Samples were characterized by high-resolution x-ray diffraction near the (004) reflection. The results are shown in Fig. 3. The peaks near −10000 arc sec are associated with the 1.5 μm AlGaSb buffer layers. Comparison to simulations indicates that the AlGaSb is 99%–100% relaxed. Previous work indicates that the dislocation density in similar layers is 10^8–$10^9/\mathrm{cm}^2$. Distinct peaks are also visible for the 12.5 nm InGaSb layers with the exception of sample A which has the smallest lattice mismatch. For samples B–E, the position of the InGaSb peaks is consistent with the nominal compositions based on reflection high-energy electron diffraction oscillations and the assumption that the layers are pseudomorphically strained to the AlGaSb buffer layer. The InGaSb peak widths are near 1300 arc sec, the value obtained from simulations. For sample F, however, the InGaSb peak is broadened and shifted, indicating partial lattice relaxation.

We performed Hall/van der Pauw transport measurements on 5×5 mm^2 squares at 300 and 77 K with magnetic fields of 0.37 and 1.0 T. In Fig. 4(a), we plot the room-temperature hole mobilities as a function of channel composition. For comparison, we also include data from the literature[10,11] for GaSb and InGaSb-channel quantum wells.

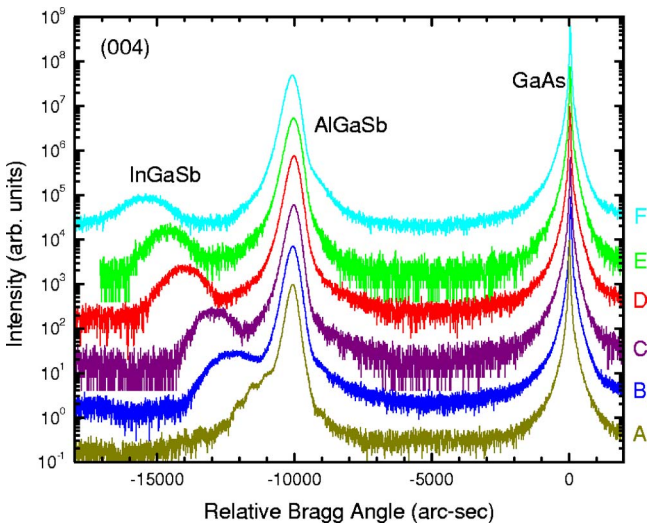

FIG. 3. (Color online) High-resolution x-ray diffraction θ-2θ scans near the (004) reflection for structures with 12.5 nm channels and varying channel composition.

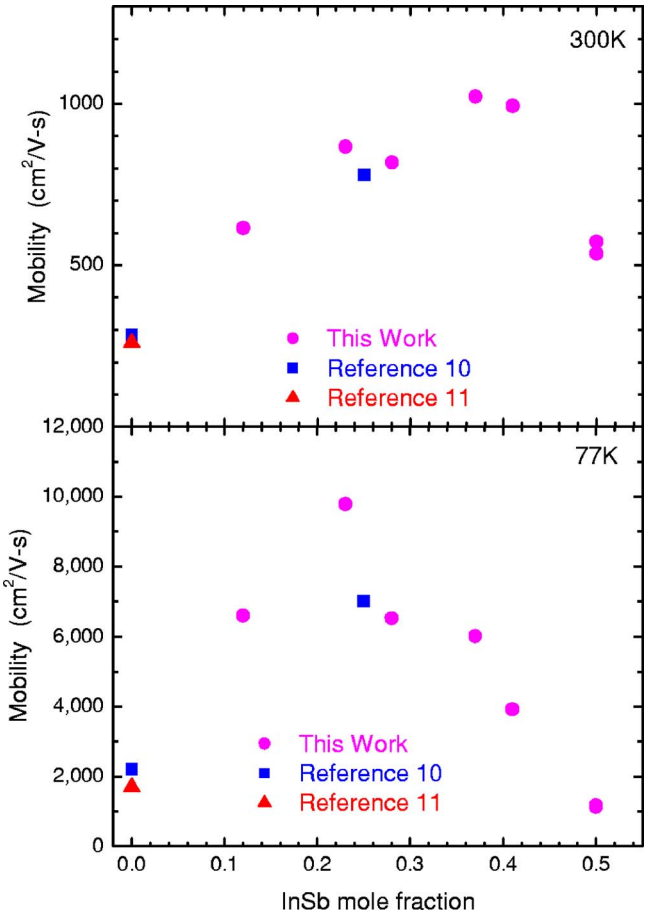

FIG. 4. (Color online) Mobility vs x for 12.5 nm $In_xGa_{1-x}Sb$ channels: (a) 300 K and (b) 77 K. The room-temperature sheet density for the InGaSb samples was $1.1\pm0.2\times10^{12}$ cm^{-2}.

As discussed above, increasing strain (and confinement) should also reduce the effective mass and enhance the mobility. We see a peak in mobility near 1000 cm^2/V s for $x\sim0.36$–0.41. For $x=0.50$, the mobility drops to ~550 cm^2/V s. This is consistent with the x-ray results which showed lattice relaxation for $x=0.50$. At 77 K [Fig. 4(b)], we observe a peak in mobility at $x=0.23$ with 9800 cm^2/V s. A possible explanation is that the low-temperature mobility is more sensitive to the formation of misfit dislocations in the strained channel than the room-temperature mobility or x-ray diffraction. Another possibility is that the mobility is more strongly influenced by alloy scattering at 77 K than at 300 K because of the reduced phonon scattering.

Based on the results in Fig. 4, we chose the $In_{0.40}Ga_{0.60}Sb$ alloy for additional investigation. Because thinner channels result in larger hh-lh splitting, one might expect higher mobility as the channel is thinned below 12.5 nm. Moreover, thinner channels should have fewer misfit dislocations which could also raise the mobility. To study these questions, we grew a set of four samples with constant composition and Be dose and varying channel thickness (5, 7.5, 10, and 12.5 nm). The results are shown on Fig. 5 where we plot mobility versus sheet carrier density at 300 K. The four samples have sheet densities of $(0.9$–$1.1)\times10^{12}/\mathrm{cm}^2$. As expected, thinner channels show higher mobility with the highest value, 1170 cm^2/V s, achieved for a channel thickness of 7.5 nm. Again, this could be a result of fewer dislocations forming in the channel and increased hh-lh splitting.

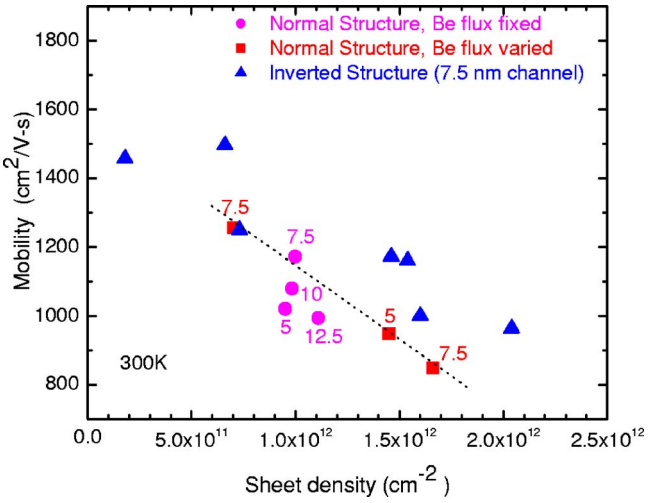

FIG. 5. (Color online) Mobility vs sheet density for $In_{0.40}Ga_{0.60}Sb$ quantum wells. The well thicknesses (in nm) are indicated for the normal structures. The well thickness was fixed at 7.5 nm for the inverted structures. The line is a guide to the eye for normal structures with 7.5 nm channels.

Although similar effects are expected for the 5 nm channel, the reduction in mobility probably results from increased interface scattering, as seen in *p*-Si.[13]

We also varied the sheet density in $In_{0.40}Ga_{0.60}Sb$ channels. A sample with no Be flux had a sheet density of $0.7\times10^{12}/cm^2$ as shown in Fig. 5. Increasing the Be flux resulted in samples with densities of $1.4\times10^{12}/cm^2$ and $1.7\times10^{12}/cm^2$. The mobility decreases as the density increases, presumably because of the effects of nonparabolicity and/or scattering as the level of occupation increases.

All the samples discussed thus far had the doping layer above the channel, as shown in Fig. 1(a). We have also investigated samples with the doping below the channel; we refer to these as inverted structures. The typical inverted structure (top to bottom) is 2 nm InAs/4 nm $In_{0.2}Al_{0.8}Sb$/10 nm $Al_{0.80}Ga_{0.20}Sb$/7.5 nm $In_{0.40}Ga_{0.60}Sb$/21 nm $Al_{0.80}Ga_{0.20}Sb$/5 nm $Al_{0.80}Ga_{0.20}Sb$(Be)/1.5 μm $Al_{0.80}Ga_{0.20}Sb$/200 nm GaAs/GaAs-SI. One advantage of an inverted structure is that smaller gate-to-channel separations can be achieved (14 nm in this case) which will allow for better aspect ratios. Another possible advantage is that the hole wave function will be moved toward the lower interface with AlGaSb. A potential disadvantage is that segregation of Be could lead to ionized impurities in the channel and a reduction in mobility. The growth procedure was modified to include an increase in temperature to 600 °C for 60 s under an Sb_2 flux between the AlGaSb lower barrier and the InGaSb channel. The temperature is then lowered to 450 °C for the channel growth. This should result in a smoother interface. A similar procedure would probably not be effective for the upper interface because the InGaSb layer could be damaged by 600 °C annealing.

Seven samples were grown with the inverted structure and are included in Fig. 5. The mobilities are generally higher than the normal structures across the full range of sheet densities. Three of the samples were grown without any intentional doping. The sheet density was $\sim0.7\times10^{12}/cm^2$ for two nominally identical samples; the mobilities were 1250 and 1500 cm^2/V s. The third undoped sample did not include an InAs cap. The mobility was 1460 cm^2/V s and the density was only $\sim0.2\times10^{12}/cm^2$ suggesting that the absence of a cap altered the surface Fermi level.

Cyclotron resonance measurements were performed on two samples to determine the effective mass. The first sample had a 12.5 nm $In_{0.23}Ga_{0.77}Sb$ channel (0.95% strain) with $n_{300}=0.89\times10^{12}/cm^2$, $\mu_{300}=870$ cm^2/V s, $n_{77}=0.78\times10^{12}/cm^2$, and $\mu_{77}=9800$ cm^2/V s. The measured effective mass was $0.101m_0$. The second sample had a 7.5 nm $In_{0.41}Ga_{0.59}Sb$ channel (2.1% strain) with $n_{300}=1.0\times10^{12}/cm^2$, $\mu_{300}=1170$ cm^2/V s, $n_{77}=1.2\times10^{12}/cm^2$, and $\mu_{77}=5600$ cm^2/V s. The measured effective mass was $0.096m_0$. For comparison, the hole effective masses for bulk GaSb and InSb are $0.40m_0$. This result confirms that strain can dramatically decrease the hole effective mass. Nonparabolicity results in higher effective masses for increasing carrier density. Klem *et al.* determined the magnitude of the effect for $In_{0.25}Ga_{0.75}Sb$ quantum wells.[10] Using their empirical relationship between effective mass and density, we estimate the second sample would have an effective mass of only $0.076m_0$ for the same density as the first sample, $0.78\times10^{12}/cm^2$. This value is similar to hole masses measured for InGaSb/GaSb quantum wells.[14] We note that these effective masses are comparable to the *electron* effective masses in GaAs or InP.

In summary, we have grown and characterized *p*-channel InGaSb quantum-well structures. Compressive strain modifies the band structure, resulting in lower effective masses and higher hole mobilities, with room-temperature values as high as 1500 cm^2/V s. Preliminary device results are promising and will be published elsewhere.[15]

This work was partially supported by the Office of Naval Research. The authors thank E. A. Aifer, C. B. Canedy, J. G. Tischler, and M. J. Yang for technical assistance and discussions.

[1]B. R. Bennett, R. Magno, J. B. Boos, W. Kruppa, and M. G. Ancona, Solid-State Electron. **49**, 1875 (2005).
[2]R. Chau, S. Datta, M. Doczy, B. Doyle, B. Jin, J. Kavalieros, A. Majumdar, M. Metz, and M. Radosavljevic, IEEE Trans. Nanotechnol. **4**, 153 (2005).
[3]P. P. Ruden, M. Shur, D. K. Arch, R. R. Daniels, D. E. Grider, and T. E. Nohava, IEEE Trans. Electron Devices **36**, 2371 (1989).
[4]G. C. Osbourn, Superlattices Microstruct. **1**, 223 (1985).
[5]M. Jaffe, J. Oh, J. Pampulapati, P. Bhattacharya, and J. Singh, Inst. Phys. Conf. Ser. No. 96, 255 (1989).
[6]M. Jaffe, J. E. Oh, J. Pamulapati, J. Singh, and P. Bhattacharya, Appl. Phys. Lett. **54**, 2345 (1989).
[7]T. J. Drummond, T. E. Zipperian, I. J. Fritz, J. E. Schirber, and T. A. Plut, Appl. Phys. Lett. **49**, 461 (1986).
[8]T. Irisawa, S. Tokumitsu, T. Hattori, K. Nakagawa, S. Koh, and Y. Shiraki, Appl. Phys. Lett. **81**, 847 (2002).
[9]M. L. Lee, E. A. Fitzgerald, M. T. Bulsara, M. T. Currie, and A. Lochtefeld, J. Appl. Phys. **97**, 011101 (2005).
[10]J. F. Klem, J. A. Lott, J. E. Schirber, S. R. Kurtz, and S. Y. Lin, J. Electron. Mater. **22**, 315 (1993).
[11]L. F. Luo, K. F. Longenbach, and W. I. Wang, IEEE Electron Device Lett. **11**, 567 (1990).
[12]K. Yoh, H. Taniguchi, K. Kiyomi, and M. Inoue, Jpn. J. Appl. Phys., Part 1 **30**, 3833 (1991).
[13]M. V. Fischetti, Z. Ren, P. M. Solomon, M. Yang, and K. Rim, J. Appl. Phys. **94**, 1079 (2003).
[14]R. J. Warburton, G. M. Sundaram, R. J. Nicholas, S. K. Haywood, G. J. Rees, N. J. Mason, and P. J. Walker, Surf. Sci. **228**, 270 (1990).
[15]J. B. Boos, B. R. Bennett, N. A. Papanicolaou, M. G. Ancona, J. G. Champlain, R. Bass, and B. V. Shanabrook, Electron. Lett. 43 (2007).